



Effects of Microwaves on Burning Velocity, UV–VIS-Spectra, and Exhaust Gas Composition of Premixed Propane Flames

Sven Eckart¹ · Sree Adinarayana Dasari^{1,2} · Elizabeth Collins^{1,3} · Ralph Behrend¹ · Julio Urbina² · Hartmut Krause¹

Received: 22 November 2021 / Accepted: 16 January 2023 / Published online: 13 February 2023
© The Author(s) 2023

Abstract

Microwaves can interact with the flame's combustion zone and increase the energy density. This induces changes to the combustion properties by influencing the radical formation and significantly expanding the flame thickness. It is possible to combust low calorific gas mixtures in a stable process without preheating or co-firing with microwave assistance. Furthermore, the hybrid heating of gaseous fuels and electrical energy offers a solution for the improved use of volatile energy sources and the further improvement of the efficiencies of thermal systems. Moreover, microwaves can be used to heat materials internally, and when coupled with external heating, contribute to a more homogeneous process. This can be particularly beneficial in the glass industry and metal processing. However, the literature on basic behaviour of this coupling such as dielectric properties for higher temperature is limited, which prevents a comprehensive evaluation of the application potential. Thus, investigations with a newly designed, externally cooled, and symmetric resonator were conducted. Furthermore, the optimized resonator was improved by installing ports for burner installation and filter elements for exhaust gas probing and optical access. An axisymmetric burner was designed to generate a steady conical laminar premixed flame, which is stabilized on the outlet of a contoured nozzle. Combustion regimes with propane/air were tested within a range of equivalence ratios from 0.9 to 1.5. Experiments were carried out with an initial temperature of 298 K under atmospheric pressure and with microwave inlet power with a range of 200 to 800 W. The optical techniques used in the current survey are based on flame contour detection using OH* chemiluminescence imaging. Additionally, spectrally resolved flame emission measurement techniques were used to monitor excited state species. Significantly increased production rates of OH*, C₂*, and CH* radicals were measured when there was an increased microwave power. The amount of NO_x and CO were increased by 20% and 55% respectively in the exhaust gas, which was determined experimentally using a probe method. Numerical simulations of the electromagnetic field and its influence on combustion were carried out to confirm these findings. This enhanced reactivity by 22%, resulted in higher burning velocity, and provided knowledge on the emission performance of the combustion process under microwave influence. The numerical electromagnetic simulations using FEKO produced results that are consistent with the experimental results.

Keywords Microwave influence · Laminar burning velocity (LBV) · Premixed flames · Exhaust gas composition (NOX/CO) · UV/VIS spectrometry

1 Introduction

In many industrial applications, liquid gas or propane is used as a pure substance in combustion processes. It is also present in a small proportion in natural gases and low calorific value gases. These processes are gaining further importance due to the partial phase-out of coal and can contribute to reducing the total carbon dioxide (CO₂) emissions. Further, the use of plasma-assisted, microwave influenced, and modified combustion has been a topic of interest for a long time (Chattock 1899). These could provide an opportunity to replace combustion gases in some cases with electric concepts, the so-called hybrid heating (Schulz et al. 2011; Heinen and O'Malley 2015). In recent years, several research groups have investigated novel approaches for the development of combustion systems (Calcote and Pease 1951) to optimize fuel and energy consumption. This study focuses on rectifying ignition (Wu et al. 2015; Wolk et al. 2013), mixing and flame stability problems (Kim et al. 2011; Altendorfner et al. 2011), and understanding and simulating fundamental physical and chemical influences. In particular, hypersonic combustion processes (Chianese et al. 2001) with devices such as plasma torches (Henriques et al. 2011; Hammack et al. 2011), microwave resonators, and other discharge technologies face complex challenges. Numerous experimental studies have applied static electric fields (Kim et al. 2011; Altendorfner et al. 2011) and microwaves (Ehn et al. 2017; Rao et al. 2011) to modify combustion processes. Therefore, the expanding blow-off and extinction limits (Jeon and Lee 2017), burning velocity (Shinohara et al. 2009; Stockman et al. 2009) and stability criteria (Jeon and Lee 2017), and soot and emission formation (Vega et al. 2007) have been investigated and analyzed. Previous work has shown that resonant microwaves interact with a hydrocarbon flame front, leading to a noticeable enhancement in laminar burning velocity (LBV) (Sullivan et al. 2004; Won et al. 2007; Tropina and Miles 2018; Tropina 2019). These observations allowed for the development of a method to measure the electric field and recalculate the laminar burning velocity (Bertrand et al. 1979). These effects were integrated into numerical models of one-dimensional laminar flames under the influence of electric fields. The results show a potential increase of energy efficiency in combined systems from electric and fuel heating. In addition, the ohmic heating seems to increase the flame temperature, which seems to be the primary mechanism for increasing the burning velocity (Chen et al. 2019). In addition, experiments were carried out with continuous microwave irradiation (Hong-Yuan and Yei-Chin 2017). They found a three-step behavior with microwave enhanced stage, thermal enhanced stage, and plasma assisted stage.

Furthermore, the field maximum of the electric field at the position of the flame was investigated (Shinohara et al. 2009; Ju et al. 2004; Stockman et al. 2006; Zaidi et al. 2005). Furthermore, the change in the emission formation of soot (Fialkov 1997), CO and NO_x have been studied in methane flames (Vega et al. 2007; Fialkov 1997). No consistent trend was found for CO and NO_x. Therefore, Ju et al. (2004) conducted a sensitivity analysis of the free electron number for different equivalence ratios. Their results indicated that the exhaust gas could absorb most of the microwave electron heating. A detailed investigation of the changed burning velocity under the influence of microwaves and using optical, spectrometric techniques and the measurement of the exhaust gas composition has not yet been carried out for propane flames. In general,

the transferability of influences from laboratory scale to industrial burners is of crucial importance. The positioning of a flame in a rectangular waveguide was investigated in a previous study (Eckart et al. 2019). This study focuses on the influences in a cylindrical combustion chamber.

Therefore, the aim of this study was (1) to gain a better understanding of the correlation between the input power of microwaves and the emissions of the premixed stabilized propane flame in the electromagnetic spectrum wavelength range of 200 to 700 nm. (2) To quantify the effect of microwave input power on the laminar burning velocity and absorption in different cavities. (3) Investigate the influence of microwaves on the emission of CO and NO_x. (4) In addition, numerical comparisons of different modified parameters were made to facilitate estimates of field geometry for industrial burner structures. In the following section, the burner method is briefly outlined, and the measurement methodology is presented. The measured change in LBV is presented as a function of the microwave power supplied and the change in the normalized optical and exhausts emissions. Further, a numerical case study for the cavity is shown.

2 Experimental Methods

2.1 Burner Setup

The burner assembly and optical measurement technology used to produce and analyze the combustion are illustrated in Fig. 1. An axisymmetric premixed burner was designed to generate a steady laminar conical premixed flame which was stabilized on the outlet of a contoured nozzle under atmospheric pressure. The shape of the axisymmetric central contracting nozzle was designed to reduce the boundary layer thicknesses by accelerating the flow and providing a flat velocity profile at the nozzle outlet. The contoured nozzle has an outlet diameter of 10 mm and an inlet length of the premixing region of 120 mm. To prevent interaction with the surrounding air, a nitrogen co-flow was installed. A flame arrestor made from ceramic material laminarized both gas mixtures. This also prevents the premixed gases from flashbacking into the pipe system. Detailed contours are given in the supplementary material SM6 and Fig. S9.

Furthermore, the gas inlets are symmetric to minimize the influence on the flame shape. An exhaust gas probe for sampling in the central axis was placed at a fixed height of 135 mm in the vertical duct. A thermocouple type K, class 1, was centrally installed to measure the exhaust gas temperature at the same height above the burner's nozzle. The aspirated exhaust gas was filtered through a membrane and dried with a water separator. After these pretreatments, NO, NO₂, and CO concentrations were measured with an exhaust gas analyzer (Testo 340). The setup uses calibrated thermal mass flow controllers (MFC, EL-Flow, Bronkhorst) for controlled fuel gas supply. They have an uncertainty of 0.8% of the reading value and 0.2% of the full-scale value. MFCs are controlled via software from a personal computer using an Ethernet connection. Air for combustion was supplied using compressed filtered air controlled by a MFC with a N₂/O₂ volume ratio of 79/21. To create a homogenous mixture of the fuel and air, a mixing chamber was used. The temperature was controlled with a thermocouple type K (d=0.5 mm) outside of the cavity. The outlet of the burner has been built into the chamber structure such that the tip of the nozzle is exactly at the base of chamber.

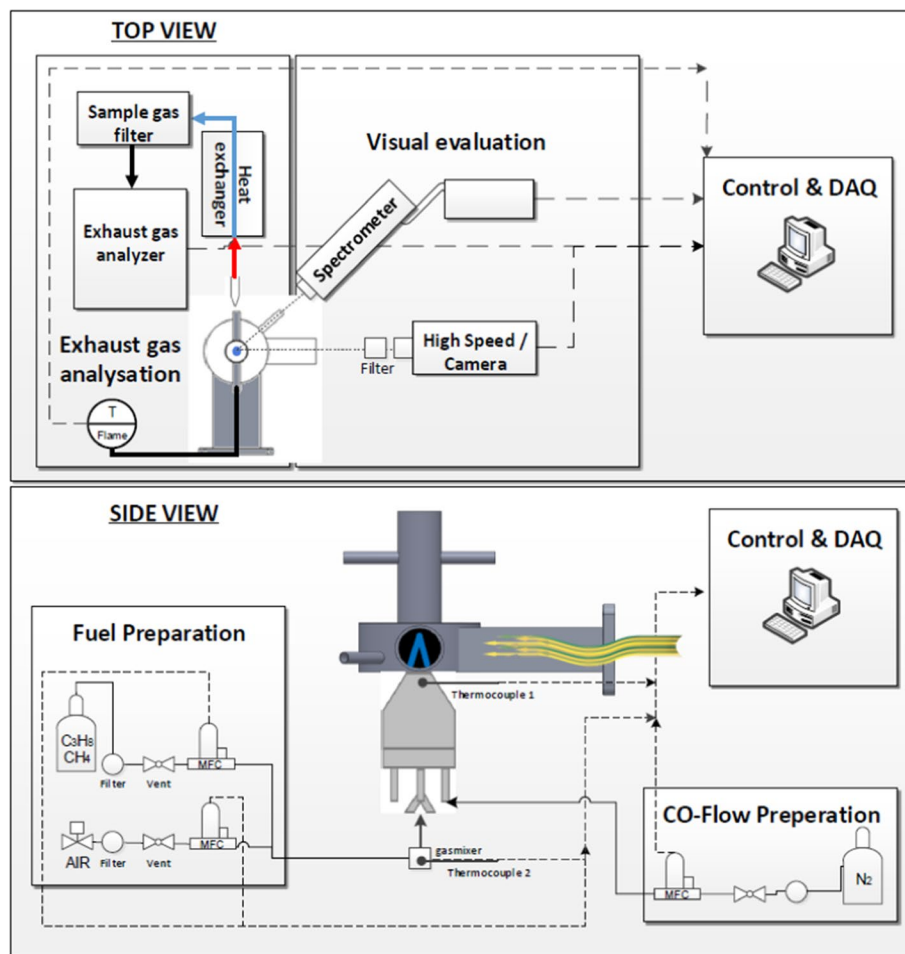


Fig. 1 Setup of the burner test rig. (top) View from the top on the experimental setup and the visual evaluation. (bottom) Side view to the gas preparation and the burner design for the premixed flame, microwave irradiation from the right side through the WR340 waveguide

2.2 Microwave Setup

A 2.45 GHz magnetron with 1200 W nominal power was connected to a WR340 waveguide via a standard launcher with an integrated cooling system. A switching power supply from ALTER (CM440) was used for continuous controllable power adjustment with a range of 120 W to a maximum of 1200 W. Microwave measurements and impedance matching were carried out using a MW2104H-260EC automatic tuner from MUEGGE. The system combines an automatic impedance and power measurement system via a 6-Port-Reflectometer with a motorized three-stub tuner for load impedance matching. The three-stub-tuner was set to automatic impedance matching with a minimum reflection coefficient as a target parameter during the experiments. The tuner was manually tuned to a specific pre-investigated point of maximum coupling in the area of the flame region. For equipment safety, a circulator was installed between the magnetron and tuner. Furthermore,

a high purity fused silica window was installed between tuner and load to ensure equipment safety against flue gas condensates or water vapor. The burner was installed in a pre-calculated, round cavity, combined with a WR340 waveguide built with high-temperature resistant steel with a diameter of $d = 45$ mm. For exhaust gas, two filters for exit and optical access, both with diameters of 40 mm and lengths of 80 mm, were installed over the burner and laterally to the burner (see Fig. 1). The burner inlet was screwed into the cavity to reduce the microwave leakage.

The cavity and the adjacent waveguide were cooled with water-cooled aluminium cooling plates and a copper spiral on the surface for safety. The setup was checked regularly for microwave leakage during its operation with a MUEGGE microwave survey meter MM3001B-110AB to comply with relevant health and safety norms.

A comparison of the input powers between the flame and the microwave power is shown in Fig. S1 of the supplementary material (SM1). To experimentally determine the electromagnetic field, a moistened thermal paper was inserted into the waveguide to check the field distribution. The arrangement can be seen in Fig. S2 of the SM2. Two reference measurements with 150 W and 200 W and 5 s of effective irradiation showed that a field distribution could be determined in Fig. S4 in the SM3.

2.3 Optical and Measurement Setup

The experimental setup was equipped with several optical measurement devices. In the current study, a technique based on the detection of OH^* in flame contours was used. The camera used to record the OH^* radical emission was an 8-bit intensified CCD camera (mvBlueFox-224G). The camera was equipped with an achromatic UV lens, combined with a short-pass optical filter centered at 307 nm. For every experimental case, 100 pictures were taken and averaged to eliminate fluctuations in the flame front. A light amplification of 6.5 was used to obtain a spherical OH^* picture. This is followed by an Abel transformation, further for each line, a local maximum point (97% intensity of the maximum in this line) analysis was performed from both sides until the middle of the flame, after which these maximum points were regressed linearly. For the calculation only the straight sections above 2 mm were used to reduce the deviations caused by the curvature of the flame next to the burner nozzle geometry. Then, the flame tip angle between both regression lines was calculated as seen in Fig. 2. In this study, the formula presented in Rallis and Garforth (1980) was used to analyze the flame cone and calculate the burning velocity, given by Eq. (1).

$$S_L = v_u \sin\left(\frac{\alpha}{2}\right) \quad (1)$$

where v_u is the unburned gas velocity at a reference temperature and α is the cone angle. The results for the LBV of propane/air were compared with previous work (Razus et al. 2012; Lowry et al. 2011; Zhou and Garner 1996; Liu and Kim 2014; Dirrenberger et al. 2011; Eckart et al. 2020) and reasonable agreement was found and can be seen in detail in Fig. S8 of the supplementary material (SM5). In addition, a spectrometer AvaSpec-ULS2048L was installed at a fixed position. This has a line of sight into the flame by means of a quartz glass fiber cable. A detailed description of the optical setup is given in Fig. 1. The spectrometer covers a wavelength range from 200 to 700 nm, with a resolution of 0.4 nm. A background superposition was done to reduce background noise. This allows for detecting a signal-to-noise ratio of 300:1 and sensitivity of 470.000 counts/ μW per ms

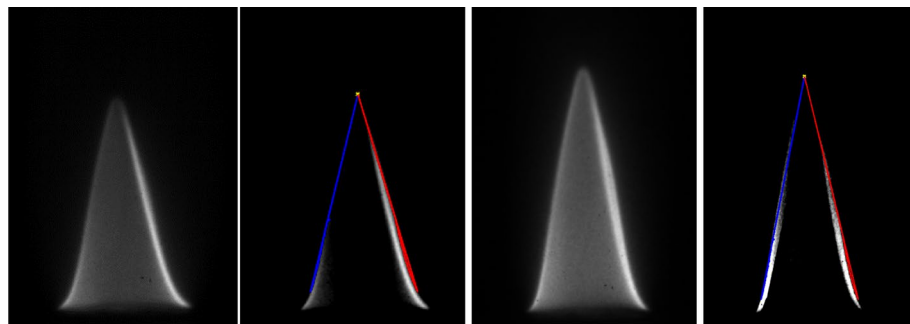


Fig. 2 Image post-processing for a propane flame (the two left images: 0.25 slm—the two right images: 0.3 slm) and an equivalence ratio of 1.1. Both flames are recorded at a microwave intensity of 300 W, left of each image pair; OH* spherical images, right of each image pair; respective Abel-inverted images with interpolated lines at the points of the local maximum are displayed

integration time. The detector has a CCD linear array with 2048×64 pixels. The lens and with the quartz glass fiber was placed 130 mm away from the center of the flame in 13 mm height above the burner nozzle. By sending light backwards through the cable, the measurement position in the combustion chamber was adjusted. A total of 300 spectra with a measurement time of 1 s were collected, integrated and averaged. A detailed description of the optical description is given in Eckart et al. (2019).

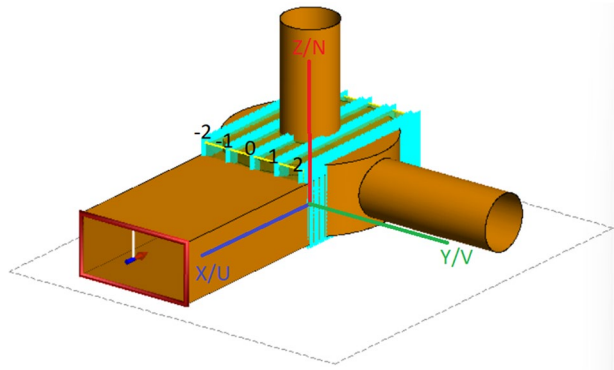
2.4 Numerical Setups

To investigate the electromagnetic field distributions in the experimental setup, several simulations were performed using computational electromagnetics software—OpenEMS (Liebig et al. 2013) and FEKO (2021). OpenEMS is a MATLAB based open-source finite-difference time-domain (FDTD) solver. The microwave cavity was constructed in OpenEMS and all the boundaries were modelled using a layer that absorbs EM waves. A 2.45 GHz microwave source was used in the experiments, so in the simulation, a sinusoidal excitation was generated at this frequency. These simulations aimed to gain a deeper understanding of the strength, propagation, and stability of the microwaves at the point where the flame would be present. Further results and explanation can be seen in the SM.

In addition to the investigations in the Matlab tool OpenEMS (Liebig et al. 2013), analyses were conducted using Altair FEKO (2021). This software package uses various methods to simulate electromagnetic problems. To simulate the near fields for the geometry shown in Fig. 3, Method of Moments (MoM) is used, considering its simple geometry and the required resolution. MoM computes a full-wave solution to Maxwell's equations, which can be used to analyze and solve scattering problems with relatively less computation time. FEKO applies this method by creating a surface mesh modeled by triangular patches to the CAD model using Rao–Wilton–Glisson (RWG) basis functions.

Further, Green's function is used to formulate a matrix equation. On using the boundary conditions, a set of linear equations are obtained where surface currents are unknowns. The system of equations is solved using LU decomposition and backward substitution to obtain a solution for the electric and magnetic currents on the triangular patches. These currents are then used to calculate both the near fields and far fields. Further details can be found at (Davidson 2011). For this experimental setup, the near fields are calculated on five planes

Fig. 3 Position of the samples in the experiment and in the numerical model for the comparison of the field distribution in the cavity



(−2, −1, 0, 1, 2), as shown in blue colour, in Fig. 3. Each of these planes contain 100 equally spaced points of measurement.

For the flame simulation, the freely propagating code of the Chemkin-PRO 2020R2 software was used. Therefore steady, and one-dimensional flames were investigated in a doubly infinite domain using the premixed laminar burner stabilized and laminar premixed flame speed code. The final results were calculated using the multi-component transport coefficients and thermal diffusion option. A typical number of grid points of around 700–1000 with respect to the gradient and curvature adaptive mesh parameters of $GRAD=0.02\text{--}0.04$ and $CURV=0.05\text{--}0.08$ were used. Further details of the simulation process are explained in Eckart et al. (2021). For the investigations, the USC II (Wang et al. 2007) reaction mechanism was used. These are validated for a wide range of conditions of H_2/CO and $C_1\text{--}C_4$ compounds.

2.5 Electromagnetic Field Distribution

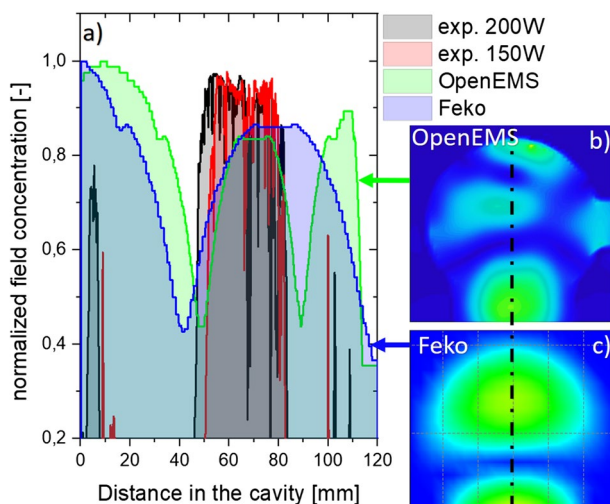
The results of the numerical investigation with FEKO and OpenEMS on the field distribution of the electromagnetic fields are shown in Fig. 4b, c. The OpenEMS simulation results in a standing wave pattern with two nodes in the cylindrical cavity and does not have a lateral symmetry. However, the FEKO simulation gives a pattern with one node and lateral symmetry, as shown in Fig. 4b, c. Additionally, the standing wave pattern is experimentally determined by placing a wet thermal paper in the cavity. When the microwaves are incident onto the cavity, the areas on the thermal paper dry up depending on the field strength of the standing wave at that location. This experiment is performed at 150 W and 200 W. The field strength obtained using the simulations and the experiment is normalized and plotted in Fig. 4a.

The wavelength of an EM wave propagating in the waveguide is different from that in free space and is given by Eqs. (2) and (3)

$$\lambda_{\text{waveguide}} = \frac{\lambda_{\text{free space}}}{\sqrt{1 - \frac{\lambda_{\text{free space}}^2}{\lambda_{\text{cutoff}}^2}}} \quad (2)$$

$$\lambda_{\text{cutoff}} = \frac{1}{2\pi\sqrt{\mu\epsilon}} \sqrt{\left(\frac{m\pi}{a}\right)^2 + \left(\frac{n\pi}{b}\right)^2} \quad (3)$$

Fig. 4 **a** Comparative electric field distribution on the axial centre axis of the cavity [marked in **b** and **c** with a dashed line], black lines in (**a**): experiment at 200 W, red lines: experiment at 150 W, blue lines: FEKO simulations and green lines: OpenEMS simulations. In **b** and **c** top view of simulation for field concentration using **b** OpenEMS, and **c** FEKO



where a and b are the cross-section dimensions of the waveguide in meters. The cut off wavelength gives the smallest wavelength that can propagate in the waveguide of given dimensions. According to these equations, the wave travels in TE_{10} mode (transverse electric mode with $m=1$ and $n=0$) at 2.45 GHz in WR 340 waveguide. The wave propagation through the cavity is similar to propagation through a waveguide with varying dimensions. The broad dimension a increases until the centre of the cavity and then decreases. Hence, $\lambda_{\text{waveguide}}$ increases until the centre and decreases until the cut-off wavelength equals the free-space wavelength, after which the waves become evanescent (Collin 1990). Considering the results from these two simulations, FEKO solution agrees with both theory and experiment. Hence, FEKO will be used for further analysis. The inconsistency in the OpenEMS solution falls beyond the scope of this paper.

3 Results and Discussion

3.1 Spectrometer Examinations

In Fig. 5a–c the results of the spectrometer examinations are displayed for specific wavelength where flame radicals (a. OH^* , 306–312 nm, b. CH^* , 428–434 nm, c. C_2^* , 510–520 nm) emit light are displayed. In subfigure (d), it was clarified that the equivalence ratio has a significant influence on the optical emission. In Fig. 5e the smoothed difference (microwave inlet power 800–0 W) for each equivalence ratio shows that the intensity of the optical emissions increases when microwaves were applied. This can be found in the supplementary Fig. S6. The OH^* radicals emitted light in the wavelengths of 307 nm and 309 nm and formed a significant double maximum peak. OH^* is typically used as a marker for the position of the flame front. The maximum OH^* ($A^2\Sigma^+ - X^2\Pi$) chemiluminescence emission that could be detected for $\phi=1.11$, which corresponds to the point of the maximum laminar burning velocity of propane, is shown in the literature (Eckart et al. 2020). The maximum electron number density is also shown there (Ju et al. 2004). Our previous publication (Eckart et al. 2019) showed a significant increase

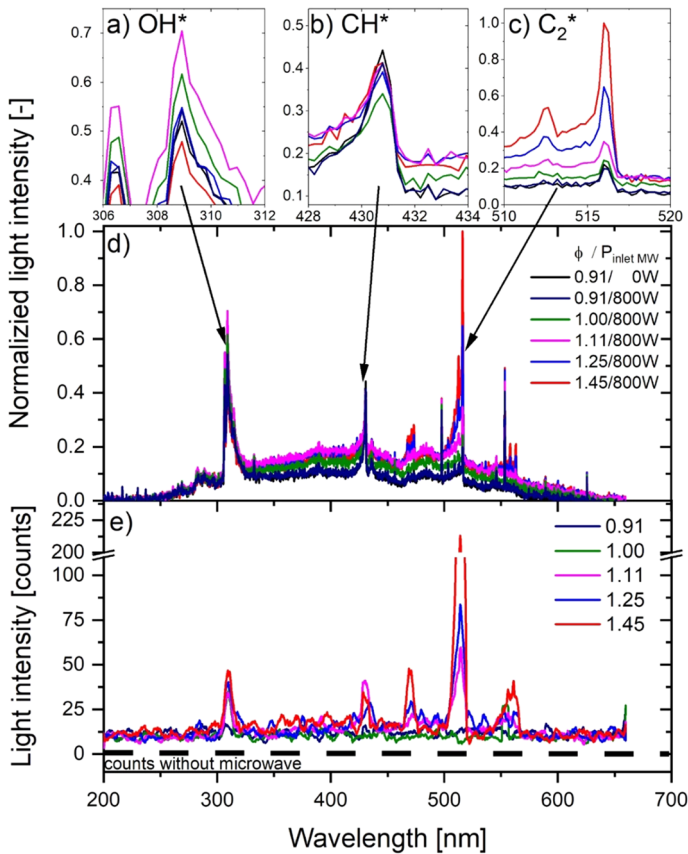


Fig. 5 Evaluation of the spectral analysis in the range from **a** 306–312 nm, **b** 428–434 nm, **c** 510–520 nm, **d** 200 nm to 650 nm at varied equivalence ratio Φ , as well as the microwave influence from 0 to 800 W and **(e)** the smoothed difference 800–0W (see Fig. S6–7 (SM4))

of OH* under the influence of microwave power with an equivalence ratio of $\phi=0.91$. An increase of $\sim 10\%$ in the absolute intensity could be determined at an input power of 600 W with a slightly different flame configuration. In the present experiments, this was tested for a broader range of equivalence ratios. The increase in intensity of OH* could be found for all equivalence ratios compared to the state of no microwave input power. To gain insight into the influencing parameters, comparative calculations for the influence of temperature on the simulated OH concentrations can be found in the Fig. S5 (SM4). It was shown that the OH increased by 10% when the inlet temperature is increased by 100 K. In addition, for the air–fuel mixture ratio resulting in the investigated equivalence ratios, it was shown that the OH concentrations varied between 0.45 and 0.7 for the normalized light intensity. Subfigure (e) shows that the effect is much stronger in the fuel-rich flames than lean flames. The heating of the unburned gases by the microwaves could thus increase the OH* concentration but does not seem to explain the total magnitude, as the adiabatic flame temperature is the highest in the stoichiometric region. In the supplementary Fig. S6, the normalized changes of the Intensity, given by $\Delta(\text{Intensity}_{800\text{W}} - \text{Intensity}_{0\text{W}})/\text{Intensity}_{\text{Max},0}$, were correlated. Moreover, the results

show that C_2^* is formed more often in the rich region, which can be attributed to a higher proportion of non-finally oxidized fuel fractions.

Subfigure (b) displays the maximal CH^* ($A^2\Delta - X^2\Pi$) light emission that was found at the wavelength 431 nm, and subfigure (c) at 516 nm the maximum peak for the Swan bands of C_2^* ($a^3\Pi_u - d^3\Pi_g$) radicals was found. These C_2^* peaks can provide further information about the possibility of forming soot and CO emissions from the ground state C_2 (Bengtsson 1996). Additionally, CH^* plays a crucial role in the oxidation process of chemically excited OH^* . The emission of CH^* does not vary as much in their normalized light intensity (factor < 1.3) as it could be seen in Fig. 5b, e. For CH^* , the maximum influence could be shown for an equivalence ratio of $\phi = 1.1$ and the rich case. These experimental results are partly different from those reported in Shinohara et al. (2009), where no changes of the CH^* and OH^* emission could be found. The optical spectra of both radicals were investigated under the influence of 150 W and 300 W of microwave power and at a slightly rich condition, which might lead to these differences. On the other hand, the present results are supported by the experiments in Rao et al. (2011). They found the OH^* emissions to increase between $\phi = 0.9$ and 1.1 with an increase in input microwave power. In their setup for a CH_4/O_2 flame, PLIF for the OH detection was used. This data is also supported by Wu et al. (2015) and Jeon et al. (2017). In contrast the C_2^* varied significantly with the equivalence ratio, ranging up to a factor of five of the comparative value. A close-up of the 516 nm (C_2^*) peak is shown in Fig. 5c; the maximum peak could be found in the fuel-rich cases. The changes in C_2^* were influenced by the equivalence ratio and the electric field. Figure 5e, shows that the C_2^* concentration peak at three different wavelengths (470–490 nm, 510–520 nm, and 550–570 nm). It can be concluded that the influence of microwaves on CH^* and C_2^* is more influenced in the rich region. In comparison to the case without the microwave irradiation, the pre- and post-reactions appear to change. On the other hand, it could be observed that for reactions involving the release of OH^* , an increased intensity is expected. This increase occurs on a scale that can not be explained by temperature changes in the unburned gas.

3.2 Exhaust Gas Investigations

The changes in the formation of pollutants due to the additional energy input of the microwaves are of high interest. The experimental results of the NO_x and CO exhaust gas measurements are shown in Fig. 6 for 0.325 slm and an equivalence ratio of $\phi = 1.0$. Further in Fig. 6b the enhancement of these values is shown.

The results reveal that by increasing the microwave input, the emission concentration for both species increases. The difference between the off mode and the microwave interference is highly notable. In addition, an increase in the exhaust gas temperature ($\Delta T < 20$ K) in the exhaust duct could also be measured. To avoid the influence of the temperature change, numerical simulations were carried out to determine its influence on CO formation. These results are shown in Fig. 7. Only a marginal change in the concentration can be observed for the near stoichiometric region with a change of 100 K. This reveals a minor decrease in the H_2O and CO_2 content and a minor increase in the CO and O_2 content. The assumed temperature changes are significantly higher than the changes in exhaust gas temperature with microwave irradiation.

It could be shown that the interference with higher microwave input power on pollutant formation is significantly lower. This might be attributed to the increase of reactivity due to the abundance of the radical pool and the enhanced absorption to thermal

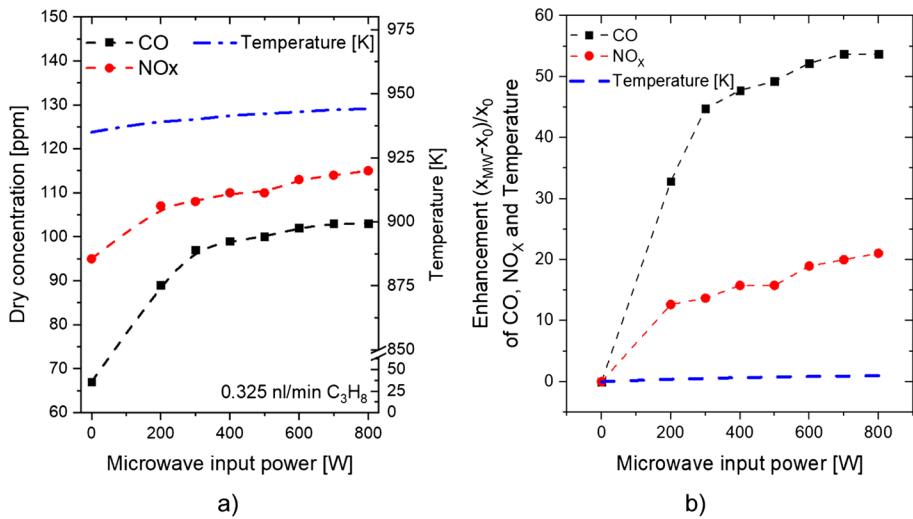
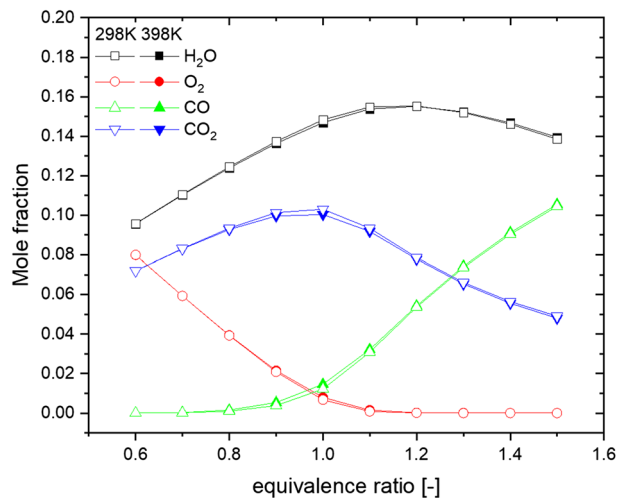


Fig. 6 **a** Measured dry concentration profiles of NO_x and CO as functions of input microwave power of propane flames at mixture temperatures $\phi=1.0$, **b** Enhancement of the concentration and temperature related to the value without microwave input power

Fig. 7 Influence of temperature on pollutant formation in propane flames—determined by USC II mechanism at 298 K and 398 K



energy. Furthermore, the temperature increases slightly at the same height. These were also addressed by Stockman et al. (2009), who found the adiabatic temperature to rise in the flame zone, indicating a higher temperature in the pre-oxidation zone. Contradictorily, Shinohara et al. could not detect any increase in temperature in his measurements and attributed the changes in the flame front to the electron density (Shinohara et al. 2009). In addition to a reduced flame height, a modified reaction sequence in the flame front is also possible. This could also cause an altered formation of emissions. Jeon and Lee investigated the liftoff of micro-jet flames and showed an increased NO_x concentration and stabilized effect with an increased input microwave power (Jeon and Lee 2017). Note that this

data set was generated for partially premixed methane flames. Figure 8 shows a further intensification of the emission formation behavior and shows their tendencies. For all the equivalence ratios tested, it can be shown that with an increased influence of microwaves NO_x and CO production rises. In addition, in the rich conditions, there is a significantly higher CO formation than in the lean conditions. These findings can be shown comprehensively in the literature (Rao et al. 2011; Zaidi et al. 2005). The increased formation of CO in the rich area correlates with the increase in C_2^* radicals, which are also shown in the spectrometer investigations. Due to the increased number of free C radicals, the possibility of further oxidation is significantly increased. This can be shown in the sensitivity analyses by Shinohara et al. (2009). The reduced NO_x emissions in the rich conditions can be attributed to a reduction in the adiabatic flame temperature and, therefore, the thermal NO_x formation. The experimental results show that the NO_x concentration is higher for combustion with microwaves than without. As the NO_x concentration tends to increase in the range of $\sim 10\%$, the effect of microwave electron heating could be one source. Consequently, it is suggested that the non-thermal effect of microwaves is small or negligible, and the effect of irradiative microwave power becomes a factor in the combustion enhancement of premixed $\text{C}_3\text{H}_8/\text{air}$ flame. Based on the NO results shown and consideration of the effect of a moderate temperature rise, this suggest that some chemical or non-thermal route is also possible.

3.3 Laminar Burning Velocity

Laminar burning velocity is one of the most important combustion parameters since it is an essential input parameter for the simulation of turbulent flame propagation. In addition, accurate laminar burning velocity measurements are of substantial interest for developing and validating chemical mechanisms. Stockman et al. (2007a, 2009) and Zaidi et al. (2005) obtained the laminar burning velocity S_L with different microwave input parameters experimentally with a flat flame method.

The results of this experimentation without microwave influence show a similar trend to the literature data, however, they are slightly lower than the previous measurement (Eckart et al. 2020) with the heat flux burner system (Li et al. 2021; Shrestha et al. 2020). The accuracy of the determined burning velocity is around $\pm 7\%$ in our measurements, the

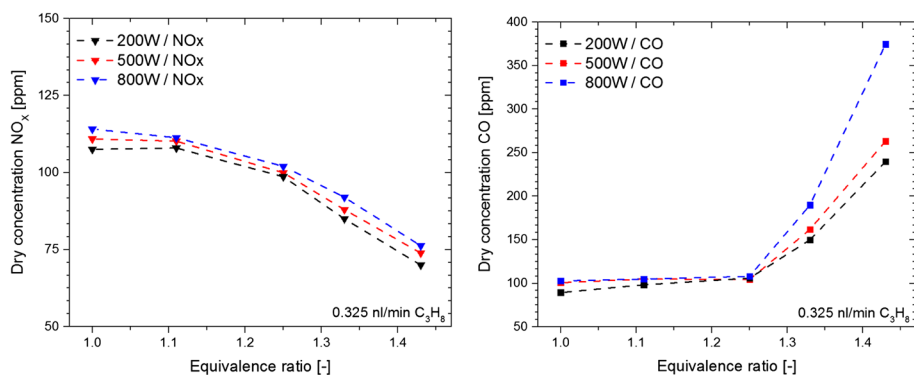


Fig. 8 Measured dry concentration profiles of NO_x and CO as functions of equivalence ratios Φ of propane flames at different input microwave power and atmospheric conditions

overall error of the method is discussed elsewhere (Walter et al. 2020; Konnov et al. 2018; Egolfopoulos et al. 2014). The uncertainty primarily depends on the fluctuations of the flame tip during the experiment, which leads to an uncertainty of the flame angle, even if this was calculated only from the middle area of the slopes. In addition, the microwave absorption by the flame and unburnt gases is subject to temporal fluctuations. For higher precision, a heat flux setup can be integrated into the cavity, which was reported in Nilsson et al. (2019).

The LBV behavior for varied microwave input power is presented in Fig. 9a. The increase of the laminar burning velocity due to the microwave influence is shown. The shortened flame length and increase in flame peak angle increase the burning velocity in flames. The shortened flame length can be interpreted as an increase in propane gas consumption in the flame closer to the burner nozzle. The results for a propane flame with three equivalence ratios of $\phi = 0.91$, 1.0, and 1.11 and a fuel stream of 0.30 slm are shown. It was observed that with a higher microwave input power, the flame propagates faster. The enhancement in Fig. 9b seems to follow the non-linear trend. It increases slightly beyond for the equivalence ratio of 1.11 beyond 400 W, beyond 500 W at $\phi = 1.0$ and beyond 550 W at $\phi = 0.91$, respectively. This implies that higher input power is necessary for leaner mixtures to generate a notable effect for a faster combustion process.

The maximum enhancement can be found at around 22%, which is comparable to the literature data (Rao et al. 2011; Jeon and Lee 2017). Their results varied from 10 to 35% for the same microwave input power (Shinohara et al. 2009; Stockman et al. 2006, 2007b).

Simulations were carried out to investigate the thermal influence on the adiabatic temperature (see Fig. 10a) and the increase in burning velocities (see Fig. 10b). As expected, the results show a significant influence on the inlet temperature. The adiabatic temperature is slightly affected by the equivalence ratio. However, the LBV enhancement does not depend on equivalence ratio. It can be observed that a maximum LBV increase of 10% is achieved with an increased inlet temperature of 20 K. This is significantly less than the measured increase in burning velocity in the cone flames. Further, if the adiabatic temperature is changed by $\Delta T = 20$ K the effect is in the range of 19–24% enhancement. Inverted, the inlet temperature in these cases must be increased up to 333–343 K. This means that a

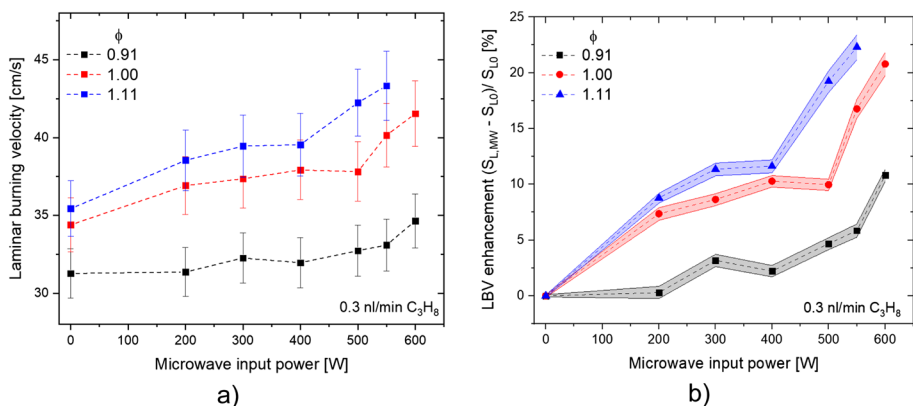
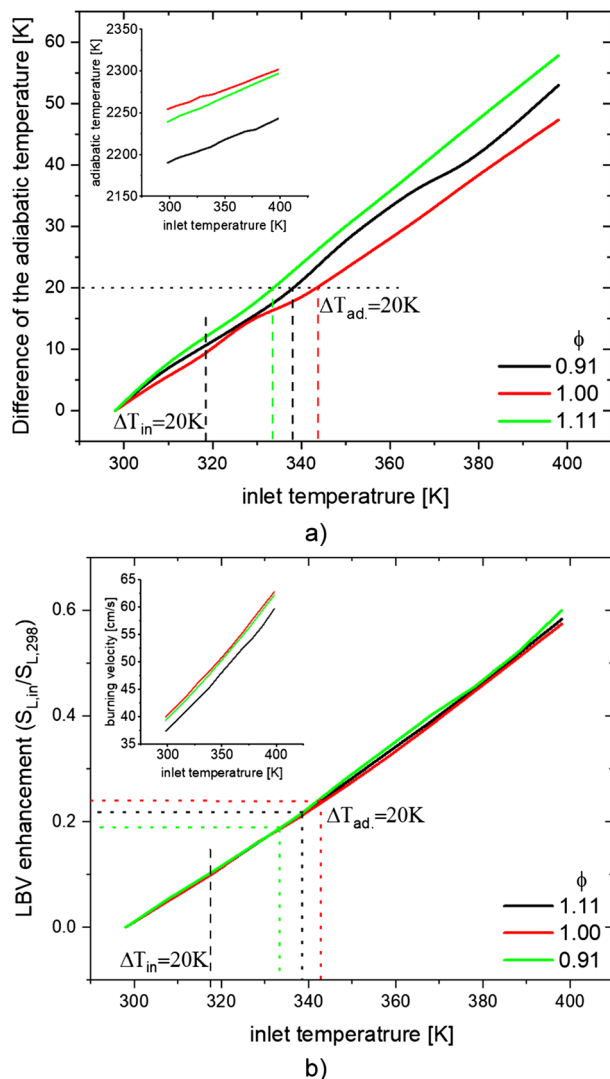


Fig. 9 **a** Increase of the laminar burning velocity of propane under the influence of varied microwaves input power at different equivalence ratios. **b** Enhancement of the laminar burning velocity in percent related to the value without microwave input power. The coloured surfaces representing the area of uncertainty

Fig. 10 **a** Numerical results (USC II) for the temperature behaviour of propane/air flames for different equivalence ratios and adiabatic temperatures, **b** normalized increments of the burning velocity with temperature compared to inlet and adiabatic temperature chances of $\Delta T = 20$ K



purely thermal influence on the acceleration is unlikely. Tropina and Miles (2018) showed numerically that the rate constant is dependent significantly on the electron temperature. This could also be proved for a wide range of equivalence ratios. Additionally, joule heating caused by the electric field in the preheated flame zone was considered for the calculations of the singlet oxygen formation. This effect would be more substantial in the fuel-rich conditions. Furthermore, Chen et al. (2019) presented a mechanism, which took the electron–ion recombination rates into account. This and the partly effect of ohmic heating were shown to be the parameters with the highest impact on the LBV enhancement. The energy lost by electrons to neutral molecules results in ohmic heating (Bisetti and Morsli 2014). The increase in mixture temperature accelerates the neutral chemical reactions as Bisetti and El Morsli pointed out. They also found a correlation to the local water vapour in the reaction zone.

3.4 Parameter Study Using FEKO

Several factors relating to the geometry of the experimental setup and microwave properties can affect the field concentration in the cavity. To investigate these effects, a parameter study was carried out for the diameter, frequency, and length of the waveguide.

The parameter study results for the diameter, as shown in Fig. 11, suggest that the location of the peak field concentration shifts in the negative y -direction with the increasing diameter. Hence, decreasing the diameter to 90 mm will result in a uniform field around the flame. However, to facilitate data acquisition and limit the temperature of the cavity, a diameter of 120 mm was chosen.

A similar result can be observed in Fig. 12 for a varying frequency—the peak shifts in the negative y -direction as the frequency increases. Therefore, using a lower frequency can result in a symmetric field pattern. However, the frequency of operation is constrained by the cross-section dimensions of the waveguide (2.2 GHz to 3.2 GHz for WR340 waveguide). A frequency of 2.45 GHz is used since it is in the ISM band at which most magnets operate.

Varying the length of the waveguide in the direction of propagation has no effect on the electric field pattern in the cylindrical cavity, as seen in Fig. 13. This is consistent with the theory presented in Collin (1990), that the field pattern is only affected by the dimensions perpendicular to the direction of propagation. A length of 120 mm is chosen to keep the magnetron at a safe distance from the hot gasses produced in the cavity.

4 Conclusions and Outlook

In this work, the influence of microwaves on the combustion process of laminar premixed flames was experimentally investigated. Propane–air mixtures with different equivalence ratios and varying volume flows were stabilized in a newly designed nozzle burner with a specially developed microwave cavity. It could be shown that the influences in the rectangular (Eckart et al. 2019) and circular systems (this study) are similar for spectral

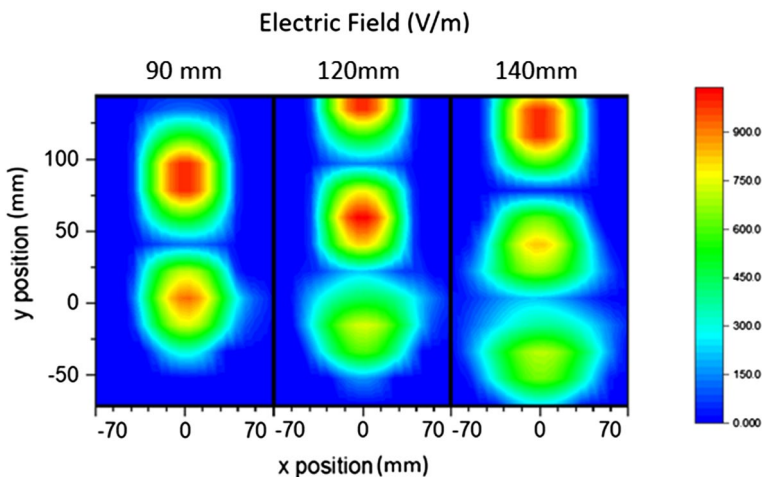


Fig. 11 Electric field for a varying cavity diameter with centre fixed at the origin

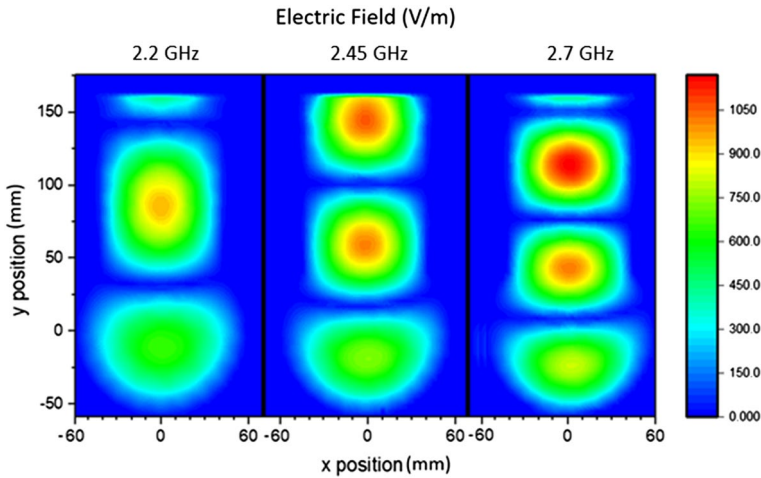


Fig. 12 Electric field for a varying frequency

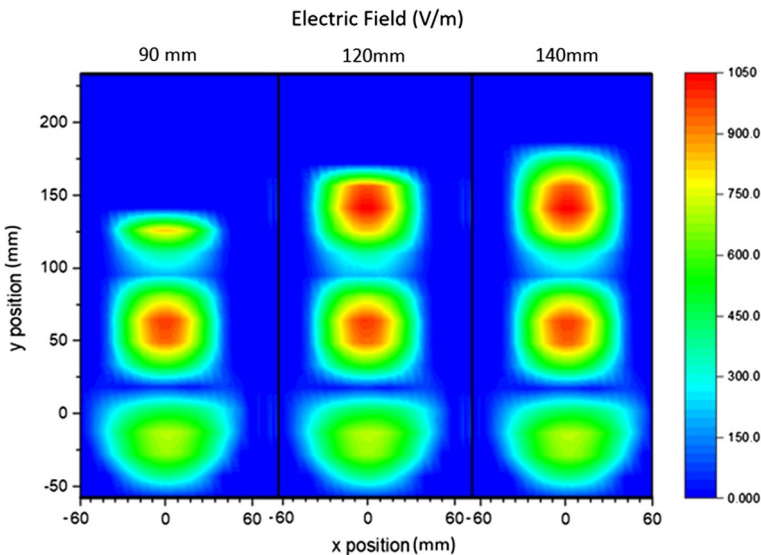


Fig. 13 Electric field for a varying waveguide length

investigations. Furthermore, it was shown that the absorption of microwave power in the flame front could significantly influence the radical formations. Through spectrometric investigation, it was determined that the microwaves increase OH^* , CH^* and C_2^* radical emission. The effects on the exhaust gas composition and the formation processes of CO, NO, and NO_2 under varying incident microwave power were analyzed, showing a slight increase in formation with increased microwave power. A combined effect of ohmic heating as a cause for higher temperatures and electron–ion recombination could explain the observations shown but could not be clearly detected by measurement.

Nevertheless, the maximum LBV and enhancement of 22% were found at the equivalence ratio of $\phi=1.1$. Additionally, the simulations and the experiment showed that the maximum field strength was not located at the position on the flame. Hence, the dimensions of the combustion chamber can be adjusted to align the maximum field strength with the flame position. For this purpose, the influence of the diameter, the frequency, and waveguide length on the field distribution were investigated. Moreover, it was found that the frequency and the diameter can be adjusted to achieve the required near field pattern. This work showed that a cylindrical cavity provides a better field distribution pattern than the rectangular cavity. Nevertheless, as shown in the paper, this is not the optimal condition. These results clearly show that can be improved in order to achieve an optimum of energy coupling and achieve a higher efficiency in hybrid heating. This procedure for non-premixed and premixed flames is still a work in progress.

Supplementary Information The online version contains supplementary material available at <https://doi.org/10.1007/s10494-023-00396-4>.

Acknowledgements The authors from Freiberg gratefully acknowledge the financial support by the European Union and the state of Saxony in the ESF project (FKZ: 100284311). The authors from New York acknowledge funding by the Pribram–Ruff Fellowship through Bates College. The authors from Penn State acknowledge funding by the RISE worldwide program of the German Academic Exchange Service (DAAD).

Funding Open Access funding enabled and organized by Projekt DEAL.

Declarations

Conflict of interest The authors declare that they have no conflict of interest.

Open Access This article is licensed under a Creative Commons Attribution 4.0 International License, which permits use, sharing, adaptation, distribution and reproduction in any medium or format, as long as you give appropriate credit to the original author(s) and the source, provide a link to the Creative Commons licence, and indicate if changes were made. The images or other third party material in this article are included in the article's Creative Commons licence, unless indicated otherwise in a credit line to the material. If material is not included in the article's Creative Commons licence and your intended use is not permitted by statutory regulation or exceeds the permitted use, you will need to obtain permission directly from the copyright holder. To view a copy of this licence, visit <http://creativecommons.org/licenses/by/4.0/>.


References

- Altendorfer, F., Kuhl, J., Zigan, L., Leipertz, A.: Study of the influence of electric fields on flames using planar LIF and PIV techniques. *Proc. Combust. Inst.* (2011). <https://doi.org/10.1016/j.proci.2010.05.112>
- Bengtsson, P.-E.: Simultaneous two-dimensional visualization of Soot and OH in flames using laser-induced fluorescence. *Appl. Spectrosc.* **50**(9), 1182–1186 (1996)
- Bertrand, C., Dussart, B., van Tiggelen, J.: Use of electric fields to measure burning velocities. *Symp. Combust.* **17**(1), 967–973 (1979)
- Bisetti, F., El Morsli, M.: Kinetic parameters, collision rates, energy exchanges and transport coefficients of non-thermal electrons in premixed flames at sub-breakdown electric field strengths. *Combust. Theory Model.* (2014). <https://doi.org/10.1080/13647830.2013.872300>
- Calcote, H.F., Pease, R.N.: Electrical properties of flames. *Burner Flames in longitudinal electric fields*. *Ind. Eng. Chem.* **43**(12), 2726–2731 (1951). <https://doi.org/10.1021/ie50504a032>
- Chattock, A.P.: On the velocity and mass of the ions in the electric wind in air. *Lond. Edinb. Dublin Philos. Mag. J. Sci.* **48**, 401–420 (1899)
- Chen, B.-S., Garner, A.L., Bane, S.P.M.: Simulation of flame speed enhancement of a hydrocarbon flame with a microwave field. *Combust. Flame* **207**, 250–264 (2019)

- Chianese, S., Fisher, K., Micci, M.: Microwave air plasma supersonic hydrocarbon combustion enhancement experiments. In: 37th Joint Propulsion Conference and Exhibit. 37th Joint Propulsion Conference and Exhibit, Salt Lake City, UT, USA, 08 July 2001–11 July 2001. American Institute of Aeronautics and Astronautics, Reston, VA (2001). <https://doi.org/10.2514/6.2001-3937>
- Collin, R.E.: Field Theory of Guided Waves IEEE Press Series on Electromagnetic Wave Theory, vol. 5. IEEE Xplore, New York (1990)
- Davidson, D.B.: Computational Electromagnetics for RF and Microwave Engineering. Cambridge University Press, Cambridge (2011)
- Dirrenberger, P., Le Gall, H., Bounaceur, R., Herbinet, O., Glaude, P.-A., Konnov, A., Battin-Leclerc, F.: Measurements of laminar flame velocity for components of natural gas. *Energy Fuels* (2011). <https://doi.org/10.1021/ef200707h>
- Eckart, S., Behrend, R., Krause, H.: Microwave influenced laminar premixed hydrocarbon flames: spectroscopic investigations. In: Proceedings 17th International Conference on Microwave and High Frequency Heating (2019). <https://doi.org/10.4995/ampere2019.2019.9834>
- Eckart, S., Cai, L., Fritsche, C., vom Lehn, F., Pitsch, H., Krause, H.: Laminar burning velocities, CO and NO_x emissions of premixed polyoxymethylene dimethyl ether flames. *Fuel* (2021). <https://doi.org/10.1016/j.fuel.2021.120321>
- Eckart, S., Fritsche, C., Krasselt, C., Krause, H.: Determining the laminar burning velocity of nitrogen diluted dimethoxymethane (OME₁) using the heat-flux burner method: numerical and experimental investigations. *Int. J. Energy Res.* **45**(2), 2824–2836 (2020)
- Egolfopoulos, F.N., Hansen, N., Ju, Y., Kohse-Höinghaus, K., Law, C.K., Qi, F.: Advances and challenges in laminar flame experiments and implications for combustion chemistry. *Prog. Energy Combust. Sci.* (2014). <https://doi.org/10.1016/j.pecs.2014.04.004>
- Ehn, A., Petersson, P., Zhu, J.J., Li, Z.S., Aldén, M., Nilsson, E.J.K., Larfeldt, J., Larsson, A., Hurtig, T., Zettervall, N., Fureby, C.: Investigations of microwave stimulation of a turbulent low-swirl flame. *Proc. Combust. Inst.* (2017). <https://doi.org/10.1016/j.proci.2016.06.164>
- FEKO: Altair (R) EM simulation software. Feko.info (Retrieved 2021)
- Fialkov, A.B.: Investigations on ions in flames. *Prog. Energy Combust. Sci.* **23**(5–6), 399–528 (1997)
- Hammack, S., Rao, X., Lee, T., Carter, C.: Direct-coupled plasma-assisted combustion using a microwave waveguide torch. *IEEE Trans. Plasma Sci.* (2011). <https://doi.org/10.1109/TPS.2011.2161778>
- Heinen, S., O'Malley, M.: Power system planning benefits of hybrid heating technologies. In: 2015 IEEE Eindhoven PowerTech. 2015 IEEE Eindhoven PowerTech, Eindhoven, Netherlands, 29 June 2015–2 July 2015, IEEE/Institute of Electrical and Electronics Engineers Incorporated, pp 1–6. (2015) <https://doi.org/10.1109/PTC.2015.7232421>
- Henriques, J., Tatarova, E., Dias, F.M., Ferreira, C.M.: Microwave N₂–Ar plasma torch. II. Experiment and comparison with theory. *J. Appl. Phys.* (2011). <https://doi.org/10.1063/1.3532056>
- Hong-Yuan, L., Yei-Chin, C.: Study of the thermal effects of microwave induced plasma on premixed methane–air flames. In: Proceedings of International Colloquium on the Dynamics of Explosions and Reactive Systems (2017)
- Jeon, Y., Lee, E.: Characteristics of liftoff and NO_x emission in microwave enhanced methane micro-jet flames. In: 11th Asia–Pacific Conference on Combustion, ASPACC 2017 (2017)
- Ju, Y., Macheret, S., Miles, R., Sullivan, D.: Numerical study of the effect of microwave discharge on the premixed methane–air flame. In: 40th AIAA/ASME/SAE/ASEE Joint Propulsion Conference & Exhibit, p. 179 (2004)
- Kim, M.K., Chung, S.H., Kim, H.H.: Effect of AC electric fields on the stabilization of premixed Bunsen flames. *Proc. Combust. Inst.* (2011). <https://doi.org/10.1016/j.proci.2010.06.062>
- Konnov, A.A., Mohammad, A., Kishore, V.R., Kim, N.I., Prathap, C., Kumar, S.: A comprehensive review of measurements and data analysis of laminar burning velocities for various fuel + air mixtures. *Prog. Energy Combust. Sci.* **68**, 197–267 (2018)
- Li, W., Mei, B., Li, Y., Eckart, S., Krause, H., Ma, S., Zhang, Y.: Insight into fuel isomeric effects on laminar flame propagation of pentanones. *Proc. Combust. Inst.* **38**(2), 2135–2142 (2021)
- Liebig, T., Rennings, A., Held, S., Erni, D.: OpenEMS—a free and open source equivalent-circuit (EC) FDTD simulation platform supporting cylindrical coordinates suitable for the analysis of traveling wave MRI applications. *Int. J. Numer. Model.* **26**, 680–696 (2013)
- Liu, Z., Kim, N.I.: An assembled annular stepwise diverging tube for the measurement of laminar burning velocity and quenching distance. *Combust. Flame* (2014). <https://doi.org/10.1016/j.combustflame.2013.11.020>
- Lowry, W., de Vries, J., Krejci, M., Petersen, E., Serinyel, Z., Metcalfe, W., Curran, H., Bourque, G.: Laminar flame speed measurements and modeling of pure alkanes and alkane blends at elevated pressures. *J. Eng. Gas Turbine Power* (2011). <https://doi.org/10.1115/1.4002809>

- Nilsson, E.J.K., Hurtig, T., Ehn, A., Fureby, C.: A setup for studies of laminar flame under microwave irradiation. *Rev. Sci. Instrum.* **90**, 113502 (2019)
- Rallis, C.J., Garforth, A.M.: The determination of laminar burning velocity. *Proc. Combust. Inst.* **6**(4), 303–329 (1980)
- Rao, X., Hemawan, K., Wichman, I., Carter, C., Grotjohn, T., Asmussen, J., Lee, T.: Combustion dynamics for energetically enhanced flames using direct microwave energy coupling. *Proc. Combust. Inst.* **33**, 3233–3240 (2011)
- Razus, D., Brinzea, V., Mitu, M., Movileanu, C., Oancea, D.: Burning velocity of propane–air mixtures from pressure–time records during explosions in a closed spherical vessel. *Energy Fuels* (2012). <https://doi.org/10.1021/ef201561r>
- Schulz, R.L., Wicks, G.G., Folz, D.C., Clark, D.E.: Overview of hybrid microwave technology. *J. South Carol. Acad. Sci.* **9**(1), 25–29 (2011)
- Shinohara, K., Takada, N., Sasaki, K.: Enhancement of burning velocity in premixed burner flame by irradiating microwave power. *J. Phys. d: Appl. Phys.* (2009). <https://doi.org/10.1088/0022-3727/42/18/182008>
- Shrestha, K.P., Eckart, S., Elbaz, A.M., Giri, B.R., Fritsche, C., Seidel, L., William, L.R., Krause, H., Mauss, F.: A comprehensive kinetic model for dimethyl ether and dimethoxymethane oxidation and NO_x interaction utilizing experimental laminar flame speed measurements at elevated pressure and temperature. *Combust. Flame* (2020). <https://doi.org/10.1016/j.combustflame.2020.04.016>
- Stockman, E.S., Zaidi, S.H., Miles, R.B., Carter, C.D., Ryan, M.D.: Measurements of combustion properties in a microwave enhanced flame. *Combust. Flame* **156**(7), 1453–1461 (2009)
- Stockman, E., Zaidi, S., Miles, R.: Pulsed microwave enhancement of laminar and turbulent hydrocarbon flames. In: 45th AIAA Aerospace Sciences Meeting and Exhibit (2006)
- Stockman, E., Zaidi, S., Miles, R.: Pulsed microwave enhancement of laminar and turbulent hydrocarbon flames. In: 45th AIAA Aerospace Sciences Meeting and Exhibit. 45th AIAA Aerospace Sciences Meeting and Exhibit, Reno, Nevada. American Institute of Aeronautics and Astronautics, Reston, VA (2007a). <https://doi.org/10.2514/6.2007-1348>
- Stockman, E., Zaidi, S., Miles, R.: Hydrocarbon flame speed enhancement with high-power pulsed microwaves. In: 38th AIAA Plasmadynamics and Lasers Conference (2007b)
- Sullivan, D., Zaidi, S.H., Macheret, S.O., Ju, Y., Miles, R.B.: Microwave techniques for the combustion enhancement of laminar flames. In: 40th AIAA Joint Propulsion Conference, pp. 3713–3727 (2004)
- Tropina, A.A.: Microwave-assisted flame with sodium seeding. *IEEE Trans. Plasma Sci.* **47**(1), 104–108 (2019)
- Tropina, A., Miles, R.B.: Combustion dynamics of microwave enhanced flame. In: 2018 AIAA Aerospace Sciences Meeting, pp. 1196–1203 (2018)
- Vega, E.V., Shin, S.S., Lee, K.Y.: NO emission of oxygen-enriched CH₄/O₂/N₂ premixed flames under electric field. *Fuel* **86**, 512–519 (2007)
- Walter, G., Wang, H., Kanz, A., Kolbasseff, A., Xu, X., Haidn, O., Slavinskaya, N.: Experimental error assessment of laminar flame speed measurements for digital chemical kinetics databases. *Fuel* (2020). <https://doi.org/10.1016/j.fuel.2020.117012>
- Wang, H., You, X., Joshi, V., Davis, G., Laskin, A., Egolfopoulos, F., Law, C.K.: USC Mech Version II. High-temperature combustion reaction model of H₂/CO/C₁–C₄ compounds. http://ignis.usc.edu/USC_Mech_II.htm (2007)
- Wolk, B., DeFilippo, A., Chen, J.-Y., Dibble, R., Nishiyama, A., Ikeda, Y.: Enhancement of flame development by microwave-assisted spark ignition in constant volume combustion chamber. *Combust. Flame* (2013). <https://doi.org/10.1016/j.combustflame.2013.02.004>
- Won, S.H., Cha, M.S., Park, C.S., Chung, S.H.: Effect of electric fields on reattachment and propagation speed of tribrachial flames in laminar coflow jets. *Proc. Combust. Inst.* **31**, 963–970 (2007)
- Wu, W., Fuh, C.A., Wang, C.: Plasma-enhanced ignition and flame stabilization in microwave plasma-assisted combustion of premixed methane/oxygen/argon mixtures. *IEEE Trans. Plasma Sci.* **43**, 3986–3994 (2015)
- Zaidi, S., Qin, X., Macheret, S., Ju, Y., Miles, R., Sullivan, D., Evans, M.: Microwave-assisted hydrocarbon flame speed enhancement. In: 43rd AIAA Aerospace Sciences Meeting and Exhibit (2005)
- Zhou, M., Garner, C.P.: Direct measurements of burning velocity of propane–air using particle image velocimetry. *Combust. Flame* (1996). [https://doi.org/10.1016/0010-2180\(96\)00002-8](https://doi.org/10.1016/0010-2180(96)00002-8)

Authors and Affiliations

Sven Eckart¹  · **Sree Adinarayana Dasari**^{1,2} · **Elizabeth Collins**^{1,3} · **Ralph Behrend**¹ · **Julio Urbina**² · **Hartmut Krause**¹

✉ **Sven Eckart**
Sven.eckart@iwtt.tu-freiberg.de

¹ Institute of Thermal Engineering, Technische Universität Bergakademie Freiberg, Freiberg, Germany

² The Pennsylvania State University, University Park, PA, USA

³ Columbia University, Manhattan, NY, USA